Critical reappraisal confirms that Mitofusin 2 is an endoplasmic reticulum–mitochondria tether

Deborah Naon[a,b], Marta Zaninello[a,c,d], Marta Giacomello[a,c], Tatiana Varanita[a,c], Francesca Grespi[a,c], Sowmya Lakshminaranayan[a,d], Annalisa Serafini[a,c], Martina Semenzato[a,c], Stephanie Herkenne[a,c], Maria Isabel Hernández-Alvarez[e], Antonio Zorzano[e], Diego De Stefani[b], Gerald W. Dorn II[f], and Luca Scorrano[a,c,1]

[a]Department of Biology, University of Padua, 35121 Padua, Italy; [b]Department of Biomedical Sciences, University of Padua, 35121 Padua, Italy; [c]Dulbecco-Telethon Institute, Venetian Institute of Molecular Medicine, 35129 Padua, Italy; [d]Fondazione S. Lucia Istituto di Ricovero e Cura a Carattere Scientifico, 00161 Rome, Italy; [e]Institute for Research in Biomedicine, 08028 Barcelona, Spain; and [f]Department of Internal Medicine, Center for Pharmacogenomics, Washington University School of Medicine, St. Louis, MO 63110

Edited by Jennifer Lippincott-Schwartz, National Institutes of Science, Bethesda, MD, and approved August 17, 2016 (received for review April 28, 2016)

The discovery of the multiple roles of mitochondria–endoplasmic reticulum (ER) juxtaposition in cell biology often relied upon the exploitation of Mitofusin (Mfn) 2 as an ER–mitochondria tether. However, this established Mfn2 function was recently questioned, calling for a critical re-evaluation of Mfn2's role in ER–mitochondria cross-talk. Electron microscopy and fluorescence-based probes of organelle proximity confirmed that ER–mitochondria juxtaposition was reduced by constitutive or acute Mfn2 deletion. Functionally, mitochondrial uptake of Ca^{2+} released from the ER was reduced following acute Mfn2 ablation, as well as in *Mfn2*$^{-/-}$ cells overexpressing the mitochondrial calcium uniporter. Mitochondrial Ca^{2+} uptake rate and extent were normal in isolated *Mfn2*$^{-/-}$ liver mitochondria, consistent with the finding that acute or chronic Mfn2 ablation or overexpression did not alter mitochondrial calcium uniporter complex component levels. Hence, Mfn2 stands as a bona fide ER–mitochondria tether whose ablation decreases interorganellar juxtaposition and communication.

mitochondria | Mfn2 | Ca^{2+} | tethering | interorganellar communication

The endoplasmic reticulum (ER) and mitochondria are physically coupled to control mitochondrial Ca^{2+} uptake, lipid transfer, autophagosome formation, ER stress, and apoptosis (1–6). Juxtaposition is mediated by protein structures that can be visualized in electron microscopy (EM) and electron tomography (ET) studies. These physical tethers span 6–15 nm when connecting smooth, and 19–30 nm when connecting rough ER to mitochondria (7). Operationally, an ER–mitochondria tether should fulfill at least these minimal criteria: (*i*) it is retrieved on the outer mitochondrial membrane (OMM); (*ii*) it is retrieved in mitochondria-associated ER membranes, the ER subdomain involved in interaction with mitochondria; (*iii*) it interacts *in trans* with a homo- or heterotypic interactor on the opposing membrane; (*iv*) its deletion increases the distance between the ER and mitochondria; or (*v*) its deletion reduces exchange of Ca^{2+} and lipids between the ER and mitochondria.

The molecular nature of ER–mitochondria tethers remained elusive for many years. The scaffold protein PACS2 (phosphofurin acidic cluster sorting protein 2) modulates their extent (8), and they include the heterotypic association between the inositol triphosphate (IP3) receptor on the ER and the OMM voltage-dependent anion channel (9). Another protein that fulfils the operational criteria to be defined as a tether is Mitofusin 2 (Mfn2). This OMM profusion protein is also retrieved in mitochondria-associated ER membranes and ER Mfn2 interacts *in trans* with Mfn1 or Mfn2 on the mitochondria to physically tether the organelles. Mfn2 ablation increases the distance between the ER and mitochondria and decreases agonist-evoked Ca^{2+} transfer from the ER to mitochondria (10) that depends on the generation of high Ca^{2+} microdomains at their interface (11, 12). The role of Mfn2 as a tether was confirmed independently in the heart (13), in pro-opiomelanocortin neurons (14), and in the liver (15). Mfn2-dependent tethering is regulated by posttranslational modifications: nondegradative Mfn2 ubiquitination by the E3 ligase MITOL reduces ER–mitochondria tethering and Ca^{2+} transfer without affecting mitochondrial or ER morphology (16). Furthermore, Mfn2 deletion impacts other facets of ER–mitochondria communication, like phosphatidylcholine (6) and cholesterol (17, 18) transfer to the mitochondria. Finally, Mfn2 was found to be specifically enriched by immunoelectron microscopy at the interface between mitochondria and the ER, as well as other organelles heterotypically tethered to the mitochondria, like melanosomes and lipid droplets (19, 20). Structurally, homo- or heterotypic *in trans* interaction between the ER–Mfn2 and mitochondrial Mfn2 or Mfn1 are supported by Mfn2's role in mitochondrial tethering and fusion (21). Mfn2 ER–mitochondria tethering function is not conserved among all eukaryotes. In the yeast *Saccharomyces cerevisiae*, the ER–mitochondria tether complex ER–mitochondria encounter structure (22) and ER membrane protein complex (23) function independently of the ancestral single yeast mitofusin and are formed by proteins located on the ER and on the OMM. Conversely, in higher nonmammalian eukaryotes Mfn2 does mediate ER–mitochondria cross-talk. For example, ER stress is a major causative component of the pathology caused by the deletion of the single *Drosophila melanogaster* mitofusin (Marf)

Significance

Organelles engage in heterotypic interactions crucial for metabolic and signaling cascades. The best-studied case of this heterotypic interaction is that between the mitochondria and endoplasmic reticulum (ER), crucial for transfer of lipids and especially Ca^{2+} between the two organelles. The original discovery that the mitochondria-shaping protein Mitofusin 2 (Mfn2) physically tethers the ER to mitochondria was recently challenged. Here, electron microscopy and fluorescent probes of organelle proximity provide definitive evidence that constitutive or acute Mfn2 ablation increases the distance between the ER and mitochondria. Functionally, this process reduces mitochondrial Ca^{2+} uptake without altering the mitochondrial Ca^{2+} uniporter complex in multiple tissues. Thus, the discoveries of the role of ER–mitochondria juxtaposition in cell biology based on Mfn2 as a tool remain unchallenged.

Author contributions: D.N., D.D.S., G.W.D., and L.S. designed research; D.N., M.Z., M.G., T.V., F.G., S.L., A.S., M.S., S.H., G.W.D., and L.S. performed research; M.G., M.I.H.-A., and A.Z. contributed new reagents/analytic tools; D.N., M.Z., M.G., T.V., F.G., S.L., A.S., M.S., S.H., and L.S. analyzed data; and D.N., G.W.D., and L.S. wrote the paper.

The authors declare no conflict of interest.

This article is a PNAS Direct Submission.

Freely available online through the PNAS open access option.

[1]To whom correspondence should be addressed. Email: luca.scorrano@unipd.it.

This article contains supporting information online at www.pnas.org/lookup/suppl/doi:10.1073/pnas.1606786113/-/DCSupplemental.

CELL BIOLOGY

(24), and Marf ablation is complemented by mammalian Mfn2 (but not Mfn1) (20, 24).

Despite evidence by multiple laboratories, Mfn2 ER–mitochondria tether function was recently challenged in two studies (25, 26). Morphometric EM analyses indicated an increase in the mitochondrial surface closely juxtaposed to the ER when Mfn2 was lost, with a corresponding increase in Ca^{2+} transfer between the two organelles when Mfn2 was acutely ablated. In cells where Mfn2 was chronically deleted, the decreased mitochondrial Ca^{2+} uptake upon agonist-mediated ER Ca^{2+} release was attributed to the reduced mitochondrial Ca^{2+} uniporter (MCU) levels. Because these studies challenge two criteria fulfilled by Mfn2 to be considered as an ER–mitochondria tether, we decided to critically re-evaluate if chronic or acute Mfn2 ablation impacts on ER–mitochondria proximity and Ca^{2+} transfer. Morphometric analysis of mitochondrial surface juxtaposition to the ER, unbiased fluorescent probes of ER–mitochondrial proximity, novel cellular models of acute Mfn2 genetic ablation, biochemical and genetic analyses of MCU complex components, and Ca^{2+} uptake measurement in purified mitochondria corroborate the wealth of evidence indicating that Mfn2 tethers the ER to mitochondria.

Results and Discussion

To compare our previous observation that Mfn2 tethers the ER to mitochondria with recent EM data questioning this result, we analyzed by EM the effect of Mfn2 ablation in mouse embryonic fibroblasts (MEFs). Visual inspection of EM images acquired by facility personnel blinded to sample identity revealed that Mfn2 and combined double *Mfn1*,Mfn2 but not *Mfn1* ablation increased the distance between ER cisternae and mitochondria. The defect was specific because reintroduction of MFN2 but not of MFN1 recovered the close juxtaposition between the two organelles (Fig. 1*A*). Tethers identified in ET span from a minimum of 9 to a maximum of 30 nm (7). We therefore measured the average distance between mitochondria and the ER located within 30 nm from the former (see Fig. S1*A* for more examples of images and presentation of how the organelles were identified). Morphometric analysis of 200 interactions per condition revealed that Mfn2 and combined double *Mfn1*,Mfn2 but not *Mfn1* ablation resulted in an ∼20% increase in the distance between the organelles, specifically recovered by MFN2 reintroduction in $Mfn2^{-/-}$ MEFs (Fig. 1*B*). This increase was also confirmed when we analyzed ER membranes located <20 nm from mitochondria (Fig. S1*B*). Our initial analysis did not correct for changes in mitochondrial surface and perimeter that could be caused by Mfn2 ablation. Mitochondrial surface increases were indeed deemed to artificially decrease Pearson's and Manders' indices of colocalization based on individual pixel channel overlap, and therefore to account for the tethering reduction measured in $Mfn2^{-/-}$ cells by confocal microscopy. As a proof of this concept, in a simulation experiment an ∼10% decrease in the Manders' coefficient was achieved by a computational ∼70% increase in the surface of the mitochondrial object. Conversely, mitochondrial surface–ER juxtaposition measured by confocal microscopy was reduced by ∼10–15% in MEFs upon Mfn2-mediated changes in mitochondrial morphology (26).

It should be mentioned that this mitochondrial surface increase was (26) or was not found (25) in EMs of $Mfn2^{-/-}$ MEFs, questioning its importance in ER–mitochondria interaction. Indeed, in cells lacking *Mfn1*, Mfn2, or both *Mfns* we always retrieved smaller mitochondria whose perimeter was reduced, challenging the concept that Mfn2 ablation increases the perimeter of the organelle (Tables S1 and S2). We nevertheless decided to take this parameter into account and devised an ER–mitochondria contact coefficient (ERMICC) that computes not only the distance between the ER and mitochondria but also the interaction length and the perimeter of the mitochondria involved in the interaction (i.e., the overall surface of the organelle) (Fig. 1*C*). ERMICC was reduced more

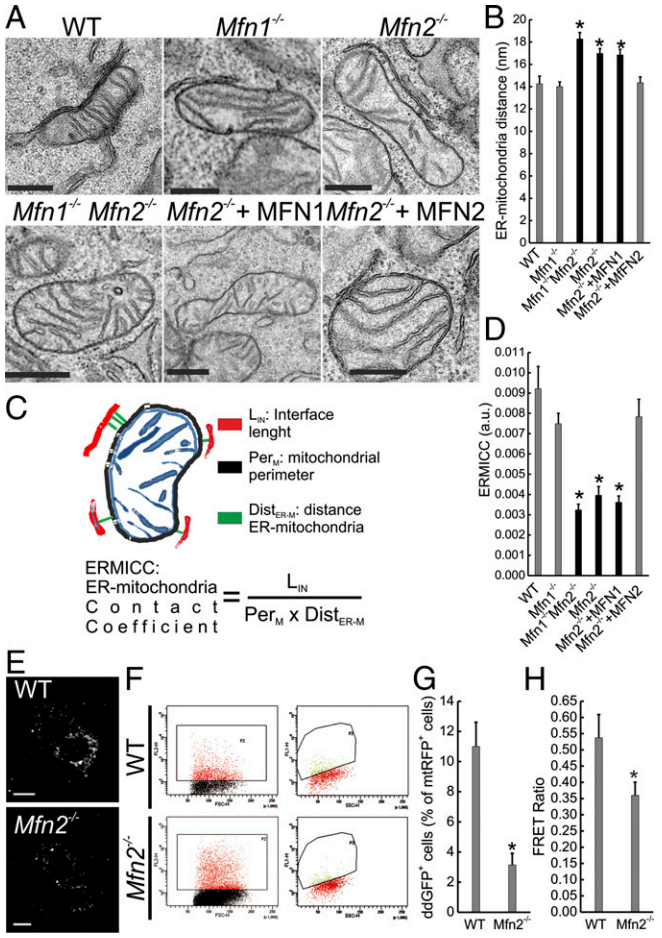

Fig. 1. Mfn2 ablation increases ER–mitochondria distance. (*A*) Representative EM images of MEFs of the indicated genotype. Where indicated, $Mfn2^{-/-}$ MEFs were cotransfected with GFP and the indicated plasmid, sorted and processed for EM. (Scale bars, 500 nm.) (*B*) Mean ± SEM of mitochondria–ER distance calculated in five independent experiments as in *A*. *$P < 0.05$ vs. WT. (*C*) A cartoon of the ERMICC contact index. (*D*) Mean ± SEM of ERMICC calculated from five independent experiments performed as in *A*. *$P < 0.05$ vs. WT. (*E*) Representative confocal images of the ER–mitochondria ddGFP fluorescence in MEFs of the indicated genotype. (Scale bars, 30 μm.) (*F*) Dot plots of ddGFP fluorescence in cells of the indicated genotype cotransfected with ddGFP monomers and cytosolic dsRED. (*Left*) Scatterplots of the gated $dsRED^+$ cells. (*Right*) $ddGFP^+$ $dsRED^+$ population. (*G*) Mean ± SEM of $ddGFP^+$ events in MEFs of the indicated genotype in three independent experiments as in *F*. *$P < 0.05$ vs. WT. (*H*) Mean ± SEM of five independent experiments of FEMP measurement of ER–mitochondria contacts in MEFs of the indicated genotype. *$P < 0.05$ vs. WT.

than 70% upon Mfn2 ablation, irrespective of whether we considered ER cisternae positioned within a 30- (Fig. 1*D*) or 20- (Fig. S1*C*) nm radius from the mitochondria. This extent of ERMICC decrease cannot be explained, even if we consider the 30% increase in mitochondrial perimeter measured in $Mfn2^{-/-}$ cells by confocal microscopy (26) but not by EM (25) (Tables S1 and S2). Indeed, fitting the formula with data from ref. 25 and with the measured increase in ER–mitochondria distance (Fig. 1*B*), ERMICC decreases by ∼30% in $Mfn2^{-/-}$ cells, indicating that the observed ERMICC reduction is the compounded effect of reduced mitochondrial surface in contact with ER and ER–mitochondria distance increase.

Finally, because tethering measurements based on EM or confocal image analysis can be prone to operator bias, we turned to assays of ER–mitochondria proximity based on GFP fluorescent probes. First, we used a dimerization-dependent (dd) GFP sensor of ER–mitochondria juxtaposition, which is formed by

two monomeric nonfluorescent green spectrum-shifted mutants of dsRED, the K_{on} of which is low enough to avoid spontaneous dimerization: one GFP is targeted to the ER surface, the other to the OMM, and when the two are closer than 20 nm a fluorescent dimer is formed (27). Live confocal imaging indicated that, as expected, ddGFP fluorescence accumulated in puncta in WT MEFs; the extent of the ddGFP puncta was greatly reduced in *Mfn2*$^{-/-}$ cells (Fig. 1*E*). To quantitate this reduction, we measured by flow cytometry the percentage of ddGFP^{+} cells in the mitochondrial dsRED^{+} [mitochondrial (mt)RFP] cell population, upon contransfection of WT and with ddGFP and mtRFP. Notably, we noted an ∼73% decrease in the population of ddGFP^{+} *Mfn2*$^{-/-}$ MEFs compared with their WT counterparts (Fig. 1 *F* and *G*). We also measured ER–mitochondria tethering using a modified FRET-based indicator of ER–mitochondria proximity (FEMP). This sensor contains a dimerization domain that allows maximal juxtaposition and FRET by brief rapamycin treatment (12). FRET intensity is inversely proportional to the sixth power of the distance between the two fluorophores and it occurs when the two FEMP fluorophores are closer than 15 nm. The modified sensor is expressed from a single mRNA that allows equimolar levels of the ER and mitochondria-anchored fluorescent proteins, thanks to the introduction of a self-cleavable viral Tav2A sequence between the two mRNAs (Fig. S2*A*). The two fluorescent proteins are appropriately targeted and measure basal as well as maximal (rapamycin-induced) organelle proximity in MEFs (Fig. S2 *B* and *C*). FRET ratios measured using the FEMP probe were significantly reduced in *Mfn2*$^{-/-}$ MEFs compared with their WT counterparts (Fig. 1*G*). In conclusion, multiple methods confirm decreased ER–mitochondria juxtaposition upon chronic Mfn2 ablation.

The morphometric, ddGFP and FEMP results complement our previous analyses of ER–mitochondria of ER–mitochondria juxtaposition based on ET, confocal microscopy, and in vitro isolated organelle interaction assays (10), and are in accordance with other EM studies that revealed decreased juxtaposition in Mfn2-deficient neurons (14) and cardiomyocytes (13). These data are difficult to reconcile with the reported tethering increase upon Mfn2 ablation (25, 26), but a potential explanation for the latter resides in the nutritional status of the cells. Stress and starvation tightens ER–mitochondria contacts (7, 28) and cell proliferation increases upon Mfn2 down-regulation (29). Indeed, we measured an increased FEMP FRET ratio (albeit still lower than the one measured in the WT counterparts) when *Mfn2*$^{-/-}$ cells were plated at higher densities (Fig. S2*D*), calling for particular care to avoid culture conditions hampering accurate estimations of interorganellar juxtaposition.

Clonal differences in established *Mfn2*$^{-/-}$ cell lines might also explain the discrepancies on Mfn2's role as a tether. We therefore decided to turn to models of Mfn2 acute ablation. Earlier observations indicated that *MFN2* gene silencing in human cells increases the distance and reduces the cross-talk between the ER and mitochondria (1, 10, 30); yet, these results required validation by unbiased fluorescent probes of ER–mitochondria proximity located only on the organelle surface and in models of Mfn2 gene ablation rather than silencing (where off-target RNAi effects might confound the interpretation of the results). We therefore measured the effect of two different shRNAs targeting Mfn2 on FRET ratios in FEMP-expressing MEFs. Normalized FRET values were comparably and significantly reduced upon silencing of Mfn2 or of the other known ER–mitochondria tether regulator *PACS2* (Fig. 2*A*), indicating that ER–mitochondria tethering decreases irrespective of whether Mfn2 is acutely or constitutively ablated. To circumvent the issue of potential shRNAs off-target effects, we then generated MEFs from conditional Mfn2 knockout (*Mfn2*$^{flx/flx}$) mice (31) and induced acute Mfn2 deletion by means of adenoviral delivery of CRE recombinase. MFN2 was reduced at 24 h postinfection and almost completely lost at 48 h (see, for example, Fig. 4*A*). In 3D reconstructions of *z*-confocal stacks of mtYFP and ER-targeted

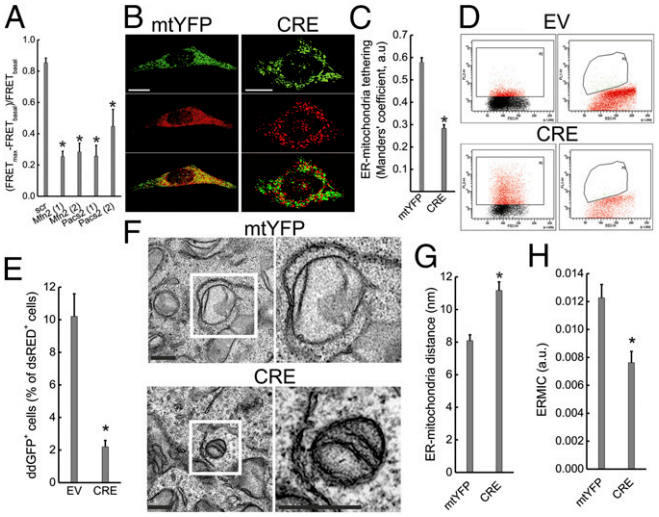

Fig. 2. Acute Mfn2 ablation increases ER–mitochondria distance. (*A*) Data represent mean ± SEM of FEMP measurement of ER–mitochondria contacts from nine independent experiments where WT MEFs were transduced with the indicated shRNA lentiviral particles for 24 h (two different shRNAs were used for Mfn2 and PACS2), transfected with FEMP, and imaged. *$P < 0.05$ vs. scramble (scr). (*B*) Volume-rendered 3D reconstructions of confocal *z*-stacks of mitochondria (*Top*, mtYFP, pseudocolored in green), ER (*Middle*, red), and merged images (*Bottom*) in *Mfn2*$^{flx/flx}$ MEFs infected with mtYFP or CRE-2A-mtYFP (CRE) adenoviruses. 24 h after infection cells were transfected ER-dsRED (pseudocolored in red) and, after an additional 24 h, imaged. (Scale bars, 30 μm.) (*C*) Data represent mean ± SEM of analysis of ER–mitochondria interaction in 10 independent experiments ($n = 10$ cells per experiment) performed as in *B*. *$P < 0.05$ vs. mtYFP. (*D*) Flow cytometry analysis of ddGFP fluorescence in *Mfn2*$^{flx/flx}$ MEFs. Cells were infected pLV-CMV (EV) or with pLV-CMV-NLSCRE (CRE) lentiviruses, cotransfected after 48 h with ddGFP monomers and cytosolic dsRED and 24 h later analyzed by flow cytometry. (*Left*) Scatterplots of the gated dsRED^{+} cells. (*Right*) GFP^{+} dsRED^{+} population. (*E*) Data represent mean ± SEM of ddGFP^{+} events in *Mfn2*$^{flx/flx}$ MEFs infected as indicated from three independent experiments as in *D*. *$P < 0.05$ vs. EV. (*F*) Representative EM images of *Mfn2*$^{flx/flx}$ MEFs infected for 48 h with mtYFP or CRE-2A-mtYFP (CRE) adenoviruses. Boxed areas are magnified 3× (*Right*). (Scale bars, 500 nm.) (*G*) Mean ± SEM of mitochondria–ER distance calculated in three independent experiments as in *F*. *$P < 0.05$ vs. mtYFP. (*H*) Mean ± SEM. ERMICC calculated from three independent experiments performed as in *G*. *$P < 0.05$ vs. mtYFP.

dsRED (ER–RFP), mitochondria and ER appeared grossly fragmented 48 h postinfection (Fig. 2*B*) and ER–mitochondria pseudocolocalization was reduced as in *Mfn2*$^{-/-}$ cells (10) (Fig. 2 *B* and *C*). Flow cytometry analysis of ddGFP fluorescence confirmed the increased ER–mitochondria distance, revealing a fivefold decrease in ddGFP^{+} events upon Cre-mediated Mfn2 ablation (Fig. 2 *D* and *E*). Finally, EM revealed that acute Mfn2 ablation increased ER–mitochondria distance (Fig. 2 *F* and *G*) and decreased the contact coefficient ERMICC (Fig. 2*H*). As for *Mfn2*$^{-/-}$ cells, these morphometric parameters were independent from the maximum distance of the tethers considered (i.e., lower than 20 or 30 nm) (Fig. S3 and Table S3). In conclusion, ER–mitochondria tethering measured by fluorescence and EM morphometry is decreased irrespective of the mean used to acutely ablate Mfn2.

If Mfn2 ablation decreases ER–mitochondria tethering, cross-talk between the two organelles should be altered, as reported by many (10, 13, 14, 16, 28). However, the key feature of reduced mitochondrial Ca^{2+} uptake following agonist induced ER Ca^{2+} release in *Mfn2*$^{-/-}$ MEFs was explained not as a consequence of lower tethering, but of lower MCU levels (26). MCU is the channel-forming subunit of the MCU holocomplex that contains other essential regulatory components, including MICU1, MICU2, and EMRE (32). In cells where Mfn2 was silenced, MCU as well as ER Ca^{2+} levels appeared normal, but mitochondrial Ca^{2+} transients were ∼40% higher, a phenotype compatible with

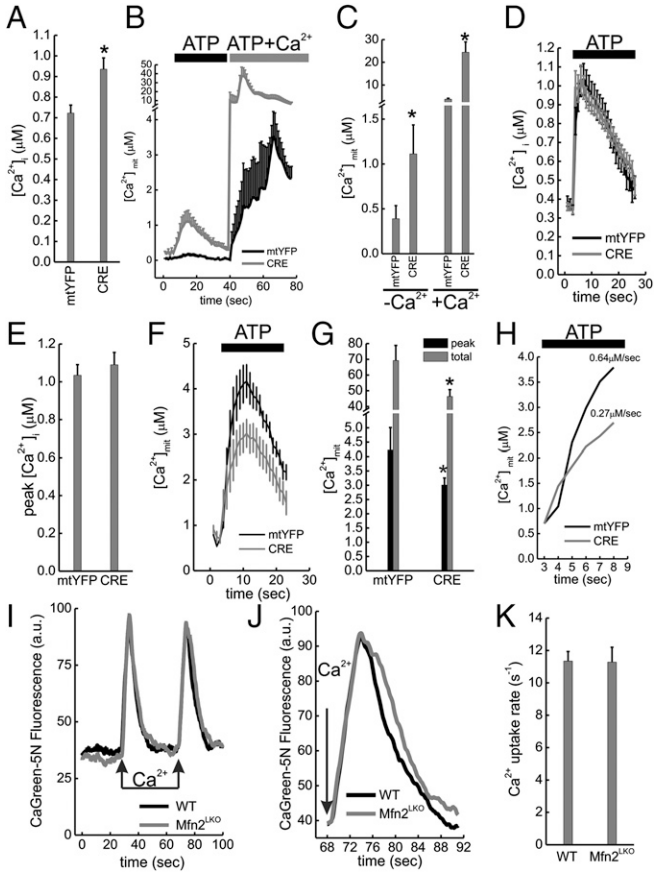

Fig. 3. Mfn2 ablation decreases mitochondrial Ca^{2+} uptake in situ but not in vitro. (*A*) Mean ± SEM of peak cytosolic Ca^{2+} concentrations ($[Ca^{2+}]_i$) in response to ATP (0.2 mM) in Ca^{2+}-free Krebbs Ringer buffer (KRB) from in three independent experiments (n = 10 recordings per experiment) where *Mfn2*$^{flx/flx}$ MEFs were infected with mtYFP or CRE-2A-mtYFP (CRE) adenoviruses and after 48 h transfected with cytAEQ. *$P < 0.05$ vs. mtYFP. (*B*) Mean ± SEM of mitochondrial Ca^{2+} ($[Ca^{2+}]_{mit}$) in Ca^{2+}-free KRB from in three independent experiments (n = 10 recordings per experiment) where *Mfn2*$^{flx/flx}$ MEFs were infected with the indicated adenoviruses and after 48 h transfected with mtAEQ. Where indicated, cells were perfused with 0.2 mM ATP and with 0.2 mM ATP + 2 mM Ca^{2+}. (*C*) Average ± SEM of peak $[Ca^{2+}]_{mit}$ from in three independent experiments (n = 10 recordings per experiment) performed as in *B*. Where indicated, cells were perfused with (+Ca^{2+}) or without (–Ca^{2+}) extracellular Ca^{2+}. *$P < 0.05$ vs. mtYFP. (*D*) Mean ± SEM of $[Ca^{2+}]_i$ from three independent experiments (n = 10 recordings per experiment) where *Mfn2*$^{flx/flx}$ MEFs were infected with the indicated adenoviruses and after 48 h transfected with cytAEQ. Cre infected cells were incubated for 30 min in Ca^{2+} free media. Where indicated, cells were perfused with 0.2 mM ATP. (*E*) Average ± SEM of peak $[Ca^{2+}]_i$ in three independent experiments performed as in *D*. (*F*) Experiments were performed as in *D* except that $[Ca^{2+}]_{mit}$ was recorded in in *Mfn2*$^{flx/flx}$ MEFs infected with the indicated adenoviruses and after 48 h transfected with mtAEQ. (*G*) Average ± SEM of three independent peak $[Ca^{2+}]_{mit}$ in experiments performed as in *F*. *$P < 0.05$ vs. the corresponding mtYFP bar. (*H*) Expanded scale of *G*. The Ca^{2+} uptake rate is indicated. (*I*) Control (WT) and liver-specific Mfn2 knockout mice (*Mfn2*^{LKO}) mitochondria (0.5 mg/mL) were incubated in experimental buffer supplemented with 1 μM CaGreen-5N and 2 μM cyclosporine A. Where indicated, 50 μM Ca^{2+} pulses were added. (*J*) Expanded scale of *I*. (*K*) Average ± SEM of $[Ca^{2+}]_{mit}$ uptake rate recorded from three couples of littermates as in *I*.

increased ER–mitochondria juxtaposition (26). To circumvent potential issues of off-target siRNA effects, we turned to our model of acute Mfn2 deletion. In the absence of extracellular Ca^{2+}, agonist-induced ER Ca^{2+} release was increased in *Mfn2*$^{flx/flx}$ infected with Cre adenoviruses (Fig. 3*A*), indicating an increase in ER Ca^{2+} stores similar to that recorded in *Mfn2*$^{-/-}$ MEFs (10). This greater availability of cytosolic Ca^{2+} resulted in increased mitochondrial Ca^{2+} uptake, which was maximized upon reintroduction of extracellular Ca^{2+} (Fig. 3 *B* and *C*), when mitochondria are exposed to capacitative Ca^{2+} entry (CCE). These data are in accordance with previous reports of increased CCE upon Mfn2 reduction (33) and require that mitochondrial Ca^{2+} uptake is measured (*i*) excluding CCE by chelating extracellular Ca^{2+} and (*ii*) exposing mitochondria to comparable Ca^{2+} levels, by titrating the IP3-coupled agonist ATP to generate the same $[Ca^{2+}]_i$ peak (Fig. 3 *D* and *E*). In these conditions, mitochondrial Ca^{2+} uptake was significantly lower (Fig. 3 *F* and *G*) and slower (Fig. 3*H*) in *Mfn2*$^{flx/flx}$ infected with Cre adenoviruses. These data are consistent with previous reports of chronic (10) and tissue-specific (13) Mfn2 ablation and can be explained by reduced ER–mitochondria juxtaposition upon acute Mfn2 deletion (see above) or by reduced intrinsic Ca^{2+} uptake ability of Mfn2-deficient mitochondria, as suggested by ref. 26. We therefore turned to purified liver mitochondria, where Ca^{2+} uptake measurements can be carried out without the confounding effects of contaminating ER [with its high Ca^{2+} affinity sarco/ER Ca^{2+}-ATPase (SERCA) pumps], by monitoring extramitochondrial Ca^{2+} insensitive to the equilibrium between the intramitochondrial stores and the targeted dye, and in the presence of the permeability transition pore-inhibitor cyclosporine A to avoid confusion from simultaneous Ca^{2+} efflux through this Ca^{2+}-sensitive nonselective inner membrane channel. Recordings of Ca^{2+} uptake and release upon pulses of Ca^{2+} were superimposable in control (WT) and Mfn2-deficient (*Mfn2*^{LKO}) liver mitochondria (Fig. 3 *I*–*K*), whose respiratory efficiency (and hence driving force for Ca^{2+} uptake) and Ca^{2+} retaining capacity were equivalent (Fig. S4). As expected from these functional results, MCU, MICU1, and MICU2 levels were not affected upon Mfn2 ablation (Fig. 4 *A*–*C*). Quantitative transcriptional analysis by RNA-sequencing of mouse hearts with cardiomyocyte-directed Mfn2 ablation (34) or overexpression (35) confirmed that uniporter holoplex component mRNAs do not change when Mfn2 is genetically manipulated (Fig. 4*D*). Accordingly, MCU, MICU1, and MICU2 levels were indistinguishable in *Mfn2*$^{-/-}$ and WT MEFs, as judged by immunoblotting (Fig. 5 *A*–*D*). Thus, genetic Mfn2 levels modulation does not affect the mitochondrial Ca^{2+} uptake machinery or process, whereas acute Mfn2 deletion decreases interorganellar tethering and mitochondrial uptake of Ca^{2+} released from the ER. To definitively test the relationship between Mfn2 ablation, MCU levels and mitochondrial Ca^{2+} uptake, we went back to WT and *Mfn2*$^{-/-}$ MEFs, where we adenovirally delivered high and comparable MCU levels (Fig. 5*D*). When agonist-induced $[Ca^{2+}]_i$ peaks were comparable (Fig. 5 *E* and *F*), mitochondrial Ca^{2+} uptake was still lower and slower in MCU overexpressing *Mfn2*$^{-/-}$ MEFs (Fig. 5 *G* and *H*). Given that no differences in mitochondrial membrane potential were measured (26), decreased ER–mitochondria tethering stands as the most probable explanation for the reduced mitochondrial Ca^{2+} uptake observed in this experiment.

Several potential explanations exist for the differences between our results and those of Filadi et al. (26): first, the cell permeabilization procedure or the concomitant presence of the ER [with active SERCA that is up-regulated in *Mfn2*$^{-/-}$ cells (10)] in the permeabilized cell preparation used in ref. 26 might affect mitochondrial Ca^{2+} uptake; second, because acute similarly to chronic Mfn2 deletion increases ER Ca^{2+} content (and hence release), ER Ca^{2+} release might not have been comparable; third, the Mfn2 siRNA used might have had potential off target effects, as highlighted by the need to predeplete ER Ca^{2+} stores in experiments of Mfn2 re-expression to obtain similar ER Ca^{2+} release (26). Finally, like tethers, levels of MCU might also be affected by cell density. We first tested this possibility in the noncycling human umbilical endothelial cells (HUVECs) where seeding density is not confounded by cell replication. Of note, MCU levels decreased proportionally to the plating density (Fig. S5*A*). A similar picture was observed in WT cells, where doubling the seeding density resulted in a 40% reduction in MCU

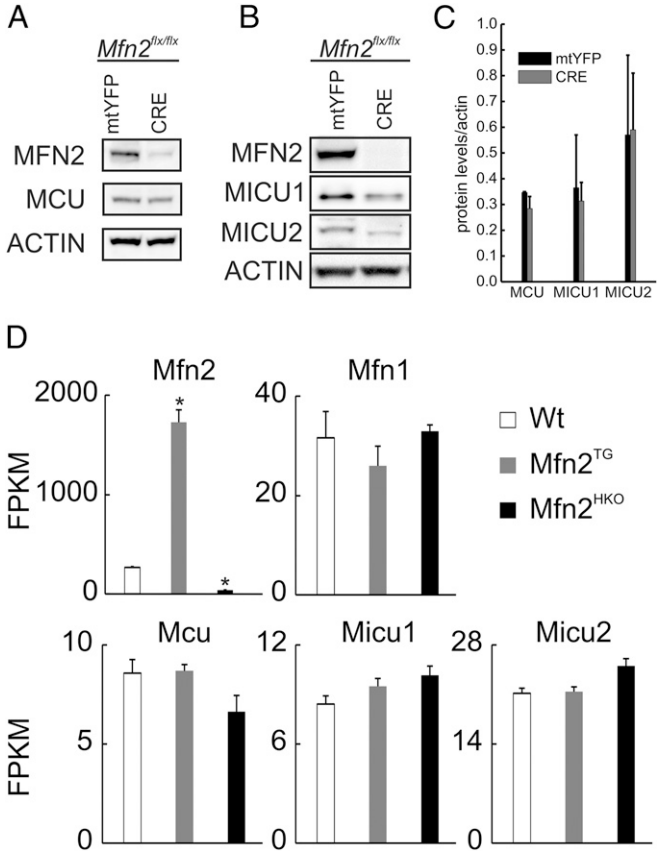

Fig. 4. Mfn2 levels do not affect components of the mitochondrial Ca^{2+} uptake machinery. (*A* and *B*) Equal amounts (40 μg) of protein were separated by SDS/PAGE and immunoblotted using the indicated antibodies from *Mfn2*$^{flx/flx}$ MEFs infected with mtYFP andCRE-2A mtYFP (CRE) adenoviruses for 48 h. (*C*) Mean ± SEM of densitometric quantification of MCU, MICU1, and MICU2 protein levels in three independent experiments as in *A*. (*D*) RNAseq results for WT, cardiomyocyte-specific Mfn2 transgenic (Mfn2^{tg}), and cardiomyocyte-directed Mfn2 knockout (Mfn2^{HKO}) mouse hearts, expressed as read fragments per kilobase of exon per million reads mapped (FPKM). *$P < 0.02$ vs. WT (one-way ANOVA).

levels. A much smaller (11%) reduction was recorded also in *Mfn2*$^{-/-}$ MEFs (Fig. S5 *B* and *C*). The discovery that density not only affects tethering (Fig. S2) but also MCU levels call for extreme caution in setting appropriate experimental conditions to inspect a potential role of a gene as a tether or as a "spacer" of the ER and mitochondria.

The critical reappraisal of Mfn2's role in ER–mitochondria juxtaposition supports previous results identifying this molecule as a physical tether between the two organelles in multiple tissues, and calls for a critical reconsideration of the conclusions of two recent papers, where limited experimental approaches were used to confute Mfn2 ER–mitochondria tethering function (25, 26). Why cells lacking Mfn2 were found to display increased ER–mitochondria juxtaposition is unclear. One possibility is that in these two papers experiments were performed on confluent or quasiconfluent cells, a "gray" zone where the tethering differences between WT and *Mfn2*$^{-/-}$ exist but are reduced, with the risk of missing them. Moreover, because MCU levels also change when cells are grown at different densities, ER–mitochondria tethering should always be measured structurally and functionally in logarithmically growing cells.

Irrespective of the reasons behind the discrepancy in the results, with previous knowledge on the function of this dynamin-related protein in membrane biology, it is difficult to rationalize the proposed role for Mfn2 as a negative regulator of tethering (26). Mfn2 was originally identified as the mitochondrial fusion factor: its overexpression clusters closely apposed individual mitochondria, indicating that it likely mediates mitochondrial adhesion (21). In a similar scenario, Mfn2 on the ER engages in homo- or heterotypic interactions with mitochondrial Mfn2 or Mfn1 to tether the two organelles. In this framework, it is not surprising that acute or chronic Mfn2 ablation decreases juxtaposition measured by EM, pseudocolocalization, FRET- or GFP-based probes, and by in vitro assays of purified ER–mitochondria cosedimentation. Functionally, transfer of Ca^{2+} from the ER to mitochondria is blunted in Mfn2-deficient cells, without any intrinsic defect in mitochondrial Ca^{2+} uptake machinery.

Mfn2 should not be considered the only mammalian tether: multiple other factors juxtapose mitochondria to the ER independently of Mfn2. The existence of Mfn2-independent tethers is confirmed by finding that the two organelles are still (albeit to a lower extent) tethered in cells lacking Mfns, and that ablation of other tethers such as PACS2 reduces FEMP-measured organelle

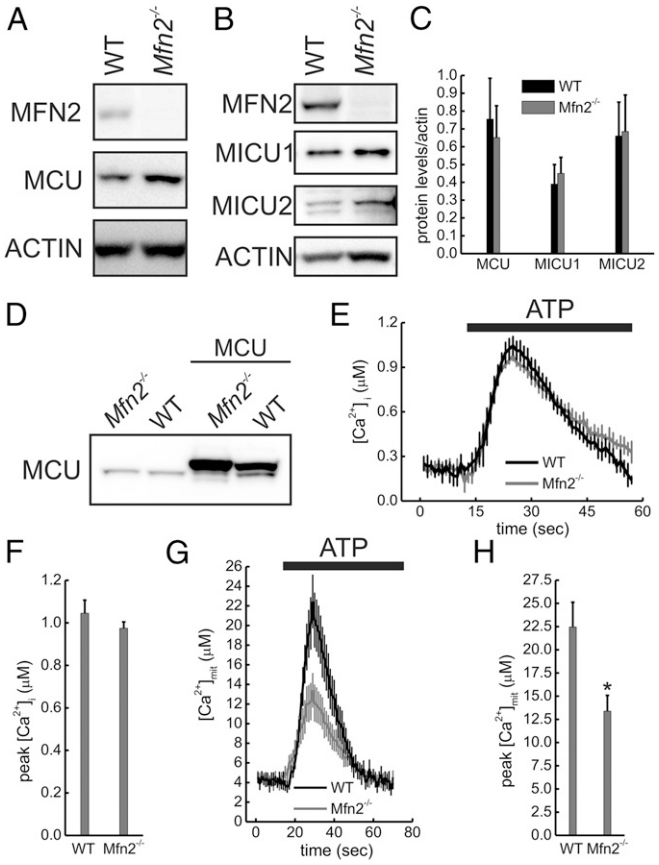

Fig. 5. Mfn2 ablation impairs mitochondrial Ca^{2+} uptake in an MCU-independent manner. (*A* and *B*) Equal amounts (40 μg) of total lysates from cells of the indicated genotypes were separated by SDS/PAGE and immunoblotted using the indicated antibodies. (*C*) Mean ± SEM of densitometric quantification of levels of the indicated MCU holoplex components from 3 to 10 independent experiments as in *A* and *B*. (*D*) MEFs of the indicated genotype were infected where indicated with MCU expressing adenoviruses and, after 48 h, were lysed and equal amount of proteins (40 μg) separated by SDS/PAGE and immunoblotted with the indicated antibodies. (*E*) Recordings of $[Ca^{2+}]_i$ in Ca^{2+}-free KRB in cells of the indicated genotypes overexpressing MCU. Where indicated, MEFs were perfused with 0.2mM (WT) or 10 μM (*Mfn2*$^{-/-}$) ATP. (*F*) Mean ± SEM of three independent experiments of peak $[Ca^{2+}]_i$ from experiments performed as in *E*. (*G*) Recordings of $[Ca^{2+}]_{mit}$ in experiments performed as in *E*. (*H*) Mean ± SEM of peak of $[Ca^{2+}]_{mit}$ from three independent experiments performed as in *G*. *$P < 0.05$ vs. WT.

CELL BIOLOGY

proximity. Finally, cross-linked complexes between Mfn2 on the ER and on the surface of mitochondria weigh more than 1 MDa (10), indicating that additional machinery is likely required on both ER and mitochondrial sides. Like Mfn2 (28), these tethers might be influenced by growth and nutrient availability (Fig. S2), as well as by progression during cell death (36), calling for their characterization and for the analysis of their role in Mfn2-dependent and independent tethering. Irrespective of the complexity of the anatomy of the ER–mitochondria interface, Mfn2 fulfills the basic criteria to stand as a bona fide tether and the discoveries on the biology of this interface based on Mfn2 stand solid.

Materials and Methods

Molecular Biology and Biochemistry. Details on plasmids and shRNA used, on the generation of MCU-Flag adenoviruses and FEMP, as well as on deep RNA sequencing are in *SI Materials and Methods*.

Cell Culture and Infection. Details on generation, immortalization, cultivation, transfection, and infection of MEFs are in *SI Materials and Methods*.

Confocal and FRET Imaging. Details on confocal microscopy imaging of live cells and FRET experiments are in *SI Materials and Methods*.

Flow Cytometry and Cell Sorting. For evaluation of ddGFP^{+} cells, MEFs were cotransfected with a cytosolic marker (cyto-dsRED), nonfluorescent GFP monomers targeted to the ER and mitochondria, and after 24 h cells were analyzed by flow cytometric analysis using a FacsCalibur Flow Cytometer (Becton Dickinson Biosciences). For sorting, 1×10^6 MEFs were cotransfected with pEGFP and the indicated plasmids and 16 h later 3×10^5 GFP^{+} cells were sorted on a FACSAria Cell Sorter (Becton Dickinson Biosciences). Details are in *SI Materials and Methods*.

Electron Microscopy. EM was performed as described previously (10). Details are in *SI Materials and Methods*.

Immunoblotting. Equal amounts of proteins were separated by 4–12% Bis-Tris SDS/PAGE (NuPAGE; Invitrogen) transferred on PVDF membranes and immunoblotted as indicated. Details are in *SI Materials and Methods*.

In Vitro Mitochondrial Assays. Mitochondrial Ca^{2+} uptake and retaining capacity were measured fluorimetrically using a Perkin-Elmer LS50B fluorimeter (λ_{ex} 505 nm; λ_{em}: 535 nm, slit 2.5 nm) in mitochondria from liver-specific Mfn2 knockout mice (*Mfn2*$^{loxP/loxP}$::Alb-Cre$^{+/-}$) and control littermates (*Mfn2*$^{loxP/loxP}$::Alb-Cre$^{-/-}$) (15). All procedures were approved by the Italian Ministry of Health (authorization 383-2015 to L.S.). Details can be found in *SI Materials and Methods*.

Aequorin Ca^{2+} Concentration Measurements. Details on reconstitution, buffer composition, and aequorin (AEQ) measurements are in *SI Materials and Methods*.

ACKNOWLEDGMENTS. We thank Drs. F. Caicci and F. Boldrin (EM Facility, Department of Biology, University of Padova) for electron microscopy. This work was supported in part by Telethon-Italy Grants GGP12162, GGP15198, and TCR02016 (to L.S.); the Associazione Italiana per la Ricerca sul Cancro Italy (to L.S.); European Research Council Grants FP7-282280 and FP7 CIG PCIG13-GA-2013-618697 (to L.S.); Ministero dell'Istruzione, dell'Università e della Ricerca Fondo per gli Investimenti della Ricerca di Base RBAP11Z3YA_005 (to L.S.); National Heart, Lung, and Blood Institute Grants R01 HL59888, R01 108943, and R01 128071 (to G.W.D.); Ministry of Economy and Competitiveness Grant SAF2013-40987R (to A.Z.); Generalitat de Catalunya 2014SGR48 (to A.Z.); Institució Catalana de Recerca i Estudis Avançats Academia (A.Z.); Centro de Investigación Biomédica en Red de Diabetes y Enfermedades Metabólicas Asociadas (A.Z.); and PIE14/00045 Instituto de Salud Carlos III (to A.Z.). L.S. is a Senior Scientist of the Dulbecco-Telethon Institute.

1. Hamasaki M, et al. (2013) Autophagosomes form at ER-mitochondria contact sites. *Nature* 495(7441):389–393.
2. Muñoz JP, et al. (2013) Mfn2 modulates the UPR and mitochondrial function via repression of PERK. *EMBO J* 32(17):2348–2361.
3. Szalai G, Krishnamurthy R, Hajnóczky G (1999) Apoptosis driven by IP(3)-linked mitochondrial calcium signals. *EMBO J* 18(22):6349–6361.
4. Rizzuto R, Brini M, Murgia M, Pozzan T (1993) Microdomains with high Ca2+ close to IP3-sensitive channels that are sensed by neighboring mitochondria. *Science* 262(5134):744–747.
5. Rizzuto R, et al. (1998) Close contacts with the endoplasmic reticulum as determinants of mitochondrial Ca2+ responses. *Science* 280(5370):1763–1766.
6. Hailey DW, et al. (2010) Mitochondria supply membranes for autophagosome biogenesis during starvation. *Cell* 141(4):656–667.
7. Csordás G, et al. (2006) Structural and functional features and significance of the physical linkage between ER and mitochondria. *J Cell Biol* 174(7):915–921.
8. Simmen T, et al. (2005) PACS-2 controls endoplasmic reticulum-mitochondria communication and Bid-mediated apoptosis. *EMBO J* 24(4):717–729.
9. Szabadkai G, et al. (2006) Chaperone-mediated coupling of endoplasmic reticulum and mitochondrial Ca2+ channels. *J Cell Biol* 175(6):901–911.
10. de Brito OM, Scorrano L (2008) Mitofusin 2 tethers endoplasmic reticulum to mitochondria. *Nature* 456(7222):605–610.
11. Giacomello M, et al. (2010) Ca2+ hot spots on the mitochondrial surface are generated by Ca2+ mobilization from stores, but not by activation of store-operated Ca2+ channels. *Mol Cell* 38(2):280–290.
12. Csordás G, et al. (2010) Imaging interorganelle contacts and local calcium dynamics at the ER-mitochondrial interface. *Mol Cell* 39(1):121–132.
13. Chen Y, et al. (2012) Mitofusin 2-containing mitochondrial-reticular microdomains direct rapid cardiomyocyte bioenergetic responses via interorganelle Ca(2+) crosstalk. *Circ Res* 111(7):863–875.
14. Schneeberger M, et al. (2013) Mitofusin 2 in POMC neurons connects ER stress with leptin resistance and energy imbalance. *Cell* 155(1):172–187.
15. Sebastián D, et al. (2012) Mitofusin 2 (Mfn2) links mitochondrial and endoplasmic reticulum function with insulin signaling and is essential for normal glucose homeostasis. *Proc Natl Acad Sci USA* 109(14):5523–5528.
16. Sugiura A, et al. (2013) MITOL regulates endoplasmic reticulum-mitochondria contacts via Mitofusin2. *Mol Cell* 51(1):20–34.
17. Wasilewski M, et al. (2012) Optic atrophy 1-dependent mitochondrial remodeling controls steroidogenesis in trophoblasts. *Curr Biol* 22(13):1228–1234.
18. Area-Gomez E, et al. (2012) Upregulated function of mitochondria-associated ER membranes in Alzheimer disease. *EMBO J* 31(21):4106–4123.
19. Daniele T, et al. (2014) Mitochondria and melanosomes establish physical contacts modulated by Mfn2 and involved in organelle biogenesis. *Curr Biol* 24(4):393–403.
20. Sandoval H, et al. (2014) Mitochondrial fusion but not fission regulates larval growth and synaptic development through steroid hormone production. *eLife* 3:e03558.
21. Rojo M, Legros F, Chateau D, Lombès A (2002) Membrane topology and mitochondrial targeting of mitofusins, ubiquitous mammalian homologs of the transmembrane GTPase Fzo. *J Cell Sci* 115(Pt 8):1663–1674.
22. Kornmann B, et al. (2009) An ER-mitochondria tethering complex revealed by a synthetic biology screen. *Science* 325(5939):477–481.
23. Lahiri S, et al. (2014) A conserved endoplasmic reticulum membrane protein complex (EMC) facilitates phospholipid transfer from the ER to mitochondria. *PLoS Biol* 12(10):e1001969.
24. Debattisti V, Pendin D, Ziviani E, Daga A, Scorrano L (2014) Reduction of endoplasmic reticulum stress attenuates the defects caused by *Drosophila* mitofusin depletion. *J Cell Biol* 204(3):303–312.
25. Cosson P, Marchetti A, Ravazzola M, Orci L (2012) Mitofusin-2 independent juxtaposition of endoplasmic reticulum and mitochondria: An ultrastructural study. *PLoS One* 7(9):e46293.
26. Filadi R, et al. (2015) Mitofusin 2 ablation increases endoplasmic reticulum-mitochondria coupling. *Proc Natl Acad Sci USA* 112(17):E2174–E2181.
27. Alford SC, Ding Y, Simmen T, Campbell RE (2012) Dimerization-dependent green and yellow fluorescent proteins. *ACS Synth Biol* 1(12):569–575.
28. Sood A, et al. (2014) A Mitofusin-2-dependent inactivating cleavage of Opa1 links changes in mitochondria cristae and ER contacts in the postprandial liver. *Proc Natl Acad Sci USA* 111(45):16017–16022.
29. Bucha S, Mukhopadhyay D, Bhattacharyya NP (2015) Regulation of mitochondrial morphology and cell cycle by microRNA-214 targeting Mitofusin2. *Biochem Biophys Res Commun* 465(4):797–802.
30. Cerqua C, et al. (2010) Trichoplein/mitostatin regulates endoplasmic reticulum-mitochondria juxtaposition. *EMBO Rep* 11(11):854–860.
31. Chen H, et al. (2010) Mitochondrial fusion is required for mtDNA stability in skeletal muscle and tolerance of mtDNA mutations. *Cell* 141(2):280–289.
32. Kamer KJ, Mootha VK (2015) The molecular era of the mitochondrial calcium uniporter. *Nat Rev Mol Cell Biol* 16(9):545–553.
33. Kasahara A, Cipolat S, Chen Y, Dorn GW, 2nd, Scorrano L (2013) Mitochondrial fusion directs cardiomyocyte differentiation via calcineurin and Notch signaling. *Science* 342(6159):734–737.
34. Chen Y, Dorn GW, 2nd (2013) PINK1-phosphorylated mitofusin 2 is a Parkin receptor for culling damaged mitochondria. *Science* 340(6131):471–475.
35. Gong G, et al. (2015) Parkin-mediated mitophagy directs perinatal cardiac metabolic maturation in mice. *Science* 350(6265):aad2459.
36. Prudent J, et al. (2015) MAPL SUMOylation of Drp1 stabilizes an ER/mitochondrial platform required for cell death. *Mol Cell* 59(6):941–955.
37. Song M, Mihara K, Chen Y, Scorrano L, Dorn GW, 2nd (2015) Mitochondrial fission and fusion factors reciprocally orchestrate mitophagic culling in mouse hearts and cultured fibroblasts. *Cell Metab* 21(2):273–285.
38. Raffaello A, et al. (2013) The mitochondrial calcium uniporter is a multimer that can include a dominant-negative pore-forming subunit. *EMBO J* 32(17):2362–2376.
39. Luke G, Escuin H, De Felipe P, Ryan M (2010) 2A to the fore—Research, technology and applications. *Biotechnol Genet Eng Rev* 26:223–260.
40. Matkovich SJ, Dorn GW, 2nd (2015) Deep sequencing of cardiac microRNA-mRNA interactomes in clinical and experimental cardiomyopathy. *Methods Mol Biol* 1299:27–49.
41. Frezza C, Cipolat S, Scorrano L (2007) Organelle isolation: Functional mitochondria from mouse liver, muscle and cultured fibroblasts. *Nat Protoc* 2(2):287–295.